Science of the Total Environment 807 (2022) 150397

Contents lists available at ScienceDirect

Science of the Total Environment

journal homepage: www.elsevier.com/locate/scitotenv

Black carbon and mineral dust in snow cover across a typical city of Northeast China

Fan Zhang [a,b], Lijuan Zhang [a,*], Mingxi Pan [a,d], Xinyue Zhong [c], Enbo Zhao [a], Yifeng Wang [a], Chen Du [a]

[a] Heilongjiang Province Key Laboratory of Geographical Environment Monitoring and Spatial Information Service in Cold Regions, Harbin Normal University, Harbin 150025, Heilongjiang, China
[b] College of Tourism Management, Sanya University, Sanya 572000, Hainan, China
[c] Key Laboratory of Remote Sensing of Gansu Province, Northwest Institute of Eco-Environment and Resources, Chinese Academy of Sciences (CAS), Lanzhou, China
[d] Mohe Meteorological Bureau, Mohe 165300, Heilongjiang, China

HIGHLIGHTS

- Concentrations of BC and MD in snow of Harbin were measured.
- Contributions of BC and MD to snow albedo in urban areas were revealed.
- BC advanced snow melting by 7.9 ± 1.16 d.
- Influence of BC and MD on snowmelt in industrial, residential and suburban areas were different.

GRAPHICAL ABSTRACT

Through the observation of the snow cover, we quantitatively assessed the contents of black carbon and mineral dust in the winter snow cover of a typical city in Northeast China. We analyzed the effects of snow pollution on snow albedo and radiative forcing, and calculated the precise number of days in which the light-absorbing substances in the snow cover in this city advanced snow melting.

ARTICLE INFO

Article history:
Received 28 June 2021
Received in revised form 11 September 2021
Accepted 13 September 2021
Available online 16 September 2021

Editor: Jianmin Chen

Keywords:
Black carbon
Mineral dust
Snow albedo
Snowmelt
Harbin

ABSTRACT

Light-absorbing impurities (LAIs), including black carbon (BC) and mineral dust (MD), in snow cover reduce snow albedo and accelerate the snow melting rate, thus influencing the regional water resources, ecological environmental security, and climate change. There is still a lack of quantitative assessments of the impacts of BC and MD on snowmelt in urban areas. This study was conducted from December 2018 to March 2019. A total of 120 snow samples were collected in Harbin, Northeast China to quantitatively assess the concentration characteristics of BC and MD in snow cover in different urban polluted areas and the impacts on snow albedo, radiative forcing, and snow melting. Average concentrations of BC and MD in snow cover in Harbin were 126,121.03 ng g^{-1} and 1419.6 μg g^{-1}, respectively. Average concentrations of BC and MD in the industrial area were the highest, which were 4.06 and 3.13 times higher, respectively, than those in the suburban area. BC or MD decreased the average snow albedo by 0.3677 (58.49%) and 0.0583 (18.18%) with radiative forcing of 44.94 W m^{-2} and 7.58 W m^{-2}, respectively. BC and MD in the industrial area, residential area, and suburban area decreased the average albedo by 0.449 (59.55%), 0.3758 (45.86%), and 0.2959 (37.65%), respectively. The impacts on snow melting time in Harbin were mainly attributed to BC, which advanced snow melting by 7.9 ± 1.16 d, while MD advanced snow melting by 3.7 ± 0.9 d. Under the combined effect of BC and MD, the industrial area, residential area, and suburban area in the city experienced advanced snow melting by 9.66 ± 0.38 d, 7.97 ± 0.31 d, and 6.67 ± 0.65 d, respectively. The results can be used to assess the contribution of intense human disturbance to snow melting.

* Corresponding author.
E-mail address: zhlj@hrbnu.edu.cn (L. Zhang).

https://doi.org/10.1016/j.scitotenv.2021.150397
0048-9697/

1. Introduction

As a basic research component of cryosphere change, snow cover is a widespread type of surface coverage on the earth. High snow albedo has a significant impact on the global energy balance (Skiles et al., 2018). The fifth IPCC (Intergovernmental Panel on Climate Change) assessment report points out that the snow cover range in the Northern Hemisphere has been shrinking since the middle of the 20th century (IPCC, 2013). In particular, the snow cover period has shortened and snow melting has significantly advanced (Tedesco et al., 2009; Sadro et al., 2019). Some studies have demonstrated that snow melting has advanced in several regions of the world due to global climate change (Tahir et al., 2019; Huang et al., 2017; Wu et al., 2018). The increase in light-absorbing impurities in snow cover is one of the key factors that accelerates snow and ice melting (Xu et al., 2009; Bond et al., 2013; Painter et al., 2013; Oaida et al., 2015; Hansen and Nazarenko, 2004; Qian et al., 2009; Qu et al., 2014; Abbatt et al., 2019). The impacts of light-absorbing impurities on snow melting have attracted increasing attention. The light-absorbing impurities mainly include black carbon (BC), organic carbon (OC), and mineral dust (MD), promoting the advanced snow melting by changing snow albedo and radiative forcing. Both BC and MD in snow cover have become the most active light-absorbing impurities leading to advanced snow melting (Hu et al., 2020; Di Mauro et al., 2017; Dombrovsky and Kokhanovsky, 2019. In addition, BC is the second most important factor affecting global climate change after carbon dioxide (Forsström et al., 2009; Dou et al., 2017). Advanced snow melting has become one of the main causes of spring drought in Northeast China (Jia et al., 2017).

There are many published results on snow albedo, radiative forcing, and snow melting based on BC and MD (Kang et al., 2020; Thind et al., 2019; Menegoz et al., 2014; Ming et al., 2016; He et al., 2018; Li et al., 2018; Zhang et al., 2018; Thind et al., 2019; Nagorski et al., 2019; Zhong et al., 2021). However, the research areas are mainly concentrated in unpopulated areas such as the North and South poles, Qinghai-Tibet Plateau, glaciers, and mountainous areas while there are few studies in urban areas, which have a great impact on human activities (Wittmann et al., 2017; Doherty et al., 2014; Zhang et al., 2018; Warren, 2019; Wang et al., 2019; Paudyal et al., 2019; Zhong et al., 2019; Niu et al., 2020; Zhong et al., 2021). Research shows that the average snow albedo decreases by approximately 0.005 to 0.423 due to BC and MD in snow cover (Flanner et al., 2007; Doherty et al., 2014). The maximum albedo reduction is 0.423 due to the combined effect of BC and MD in snow cover on the northeast Qinghai-Tibet Plateau (Li et al., 2019). The average albedo caused by BC and MD in glacier snow in the southeast, the Namtso area in the central region, and Jade Dragon Snow Mountain in the south of the Qinghai-Tibet Plateau has decreased by 0.141 ± 0.02, 0.11 to 0.28, and 0.11 ± 0.03 (Niu et al., 2017), respectively. The average albedo reduction caused by BC impurities were from 0.015 to 0.016, and that caused by MD ranged from 0.0077 to 0.015, for snow grain radii of 100 μm for northern Chile, the region near Santiago, and southern Chile (Rowe et al., 2019). Certain scholars studied the impacts of snow cover on radiative forcing and agree that BC and MD in snow cover result in an increase in radiative forcing (Xie et al., 2018; Zhao et al., 2014; Torres et al., 2018; Pu et al., 2019;). The results show that BC and MD in Arctic snow cover led to the minimum radiative forcing value. The median value was less than 1 W m^{-2} (Skiles et al., 2018). The instantaneous radiative forcing of snow cover in the Sahara Desert can reach 153 W m^{-2} (Di Mauro et al., 2015). Moreover, the radiative forcing in northern China increases from 3 W m^{-2} in fresh snow to 28 W m^{-2} in old snow during spring (Dang et al., 2017).

The impacts of BC and MD on the snow melting time have been investigated (Svensson et al., 2018; Zhang et al., 2018; Niu et al., 2017; Zhong et al., 2021). For instance, BC and MD in glacier snow on the southeastern and central Qinghai-Tibetan Plateau advance snow melting by 4.56 ± 0.71 days and 3.1 ± 0.1 days, respectively (Niu et al., 2020; Niu et al., 2017). The combined effect of BC and MD in northern Xinjiang advances snow melting by 1.36 ± 0.61 to 6.12 ± 3.38 days (Zhong et al., 2019). In addition, the combined action of BC and MD in the southern Altai region resulted in a decrease in the number of snowmelt days by 3.0 ± 0.4 days (Zhong et al., 2021). In addition to natural areas, the concentration of light-absorbing impurities in urban snow cover has been studied (Kuchiki et al., 2015; Pu et al., 2017; Wang et al., 2013a, 2013b). According to Wang et al. (2013), the concentration of BC on the snow surface in the heavy industrial area of Northeast China can reach 1000 to 2000 ng g^{-1}, which is about 15 times higher than that in an area less affected by human beings (northern Xinjiang). However, research on BC and MD in urban snow cover is currently limited to the content determination and seldom includes albedo and radiative forcing.

Studies have shown that the end date of winter snow cover in Harbin has advanced and the snow cover period has shortened by about 18 days (Bo et al., 2019). Hence, the paper focuses on the impacts of light-absorbing impurities on snow albedo, radiative forcing, and snow melting time based on the analysis of BC and MD contents in urban snow in Harbin. The paper reveals the impacts and contribution of intense human disturbance on snow melting and provides a basis for studying the influence of changes in snow.

2. Materials and methods

2.1. Study area

Heilongjiang Province has the highest latitude in northern China. As the capital city of Heilongjiang Province, Harbin is located in southern Heilongjiang Province, 125°42′ E to 130°10′ E and 44°04′ N to 46°40′ N. Harbin is a major city with high latitude and low temperature in China and has a mid-temperate continental monsoon climate. The long-term average of cumulative snowfall in winter is 29 cm. The snow cover period is as long as 6 months (Ban and Sun, 2013). Harbin is the capital city with the most abundant snow cover resources in China. The concentrated snowfall period is from November to February of the following year. Harbin has a total area of 53,100 km^2, an urban area of 7086 km^2, and a municipal area of 10,198 km^2. It has jurisdiction over 18 county-level administrative regions, including 9 municipal districts, 2 county-level cities, and 7 counties. With a permanent resident population of 10.858 million, it is the most populous city in Northeast China with the largest spatial area, and Harbin is a key central city and one of the representative heavy industrial cities in Northeast China. Harbin is the most essential industrial base since the founding of the People's Republic of China. As a typical coal-burning city in winter with a heating period of half a year, Harbin is the capital city with the most serious pollution in Northeast China and even in the whole country (Wang et al., 2013a, 2013b; Chen et al., 2015; Zhou et al., 2017). Due to the serious pollution, more and more BC and MD impurities are deposited on the snow surface, and snow melt is accelerated. As an important source of spring water resources, variation in snow cover can directly affect the spring drought and water security of Harbin city.

2.2. Sample collection

Snow samples were collected from December 2018 to March 2019 in Harbin during the whole winter snow cover period in 2018. The first snowfall occurred in Harbin on December 24, 2018. Samples were collected every 15 days during the early snow period. In this study, the whole snow cover was divided into three periods: the early, stable, and melt periods. The criteria for defining different periods were based on snowfall time, temperature, and snow depth. After the first snowfall, the following 20 days were defined as the early period. The melt period was defined as the period when the daily maximum temperature in Harbin reached or exceeded 0 °C, until the complete melting of snow. The stable period was defined as the period between the early period and the melt period. In this study, the stable period was from

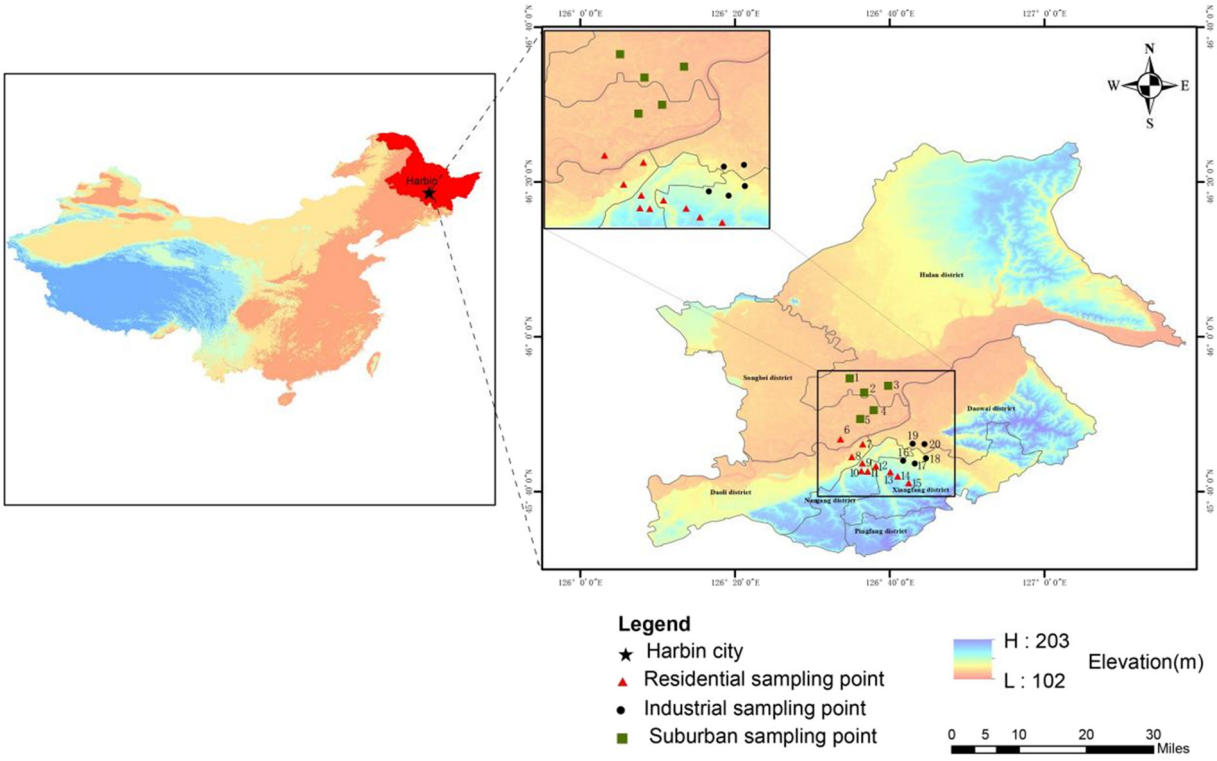

Fig. 1. Geographical locations of surface snow sampling sites across Harbin city in winter 2018.

January 13 to February 15, 2019. During the whole snow period, 6 rounds of sampling were conducted, and a total of 120 samples were collected.

In this study, 20 sampling points were selected equidistantly from north to south in the main urban area of Harbin, running through seven densely populated areas of Hulan, Songbei, Daoli, Daowai, Nangang, Xiangfang and Pingfang Districts (Fig. 1). Harbin was further divided into three functional areas in the paper, the suburban area, residential area, and industrial area. The principle of functional area division was that the suburban area was more than 3 km away from the densely populated area to ensure that it was not affected by roads, industries, and resident activities. The principle of dividing the residential area was that this was the living area of urban residents, and no industrial pollution occurred within 3 km. The industrial area was the area around Huagong Road in Harbin with a high degree of industrialization, which is a typical industrial area in Harbin.

Clean shovels were used to collect snow samples (5 cm depth) from the snow surface (Fig. 2). In addition, attention was paid to not collect debris such as leaves when sampling. Snow samples were stored in Whirl-Pak (2 L) standard sterile bags. All snow samples were kept frozen until they were filtered in the laboratory. During the process of sampling, snow depth was measured with a steel ruler. Each sampling point was measured 3 times, and the average value was calculated. The density was measured with a layered density shovel. A snow densitometer with a length, width, and height of 10 cm, 5 cm, and 5 cm, respectively, was used. The mass of the snow was measured with a balance. Then, the snow density was calculated by dividing the mass of the snow sample by the volume of the sample. The snow particle size was determined using a high-power photographic microscope (Anyty, Tianjin, China) and a snow particle size plate (manufactured by the Institute of Cold and Drought, Chinese Academy of Sciences). The measurement accuracy was 0.1 mm. After the observation, the index values were recorded.

2.3. Light-absorbing impurity analysis

The concentration of BC in snow was measured using a thermo-optic method through the DRI Model 2015 multi-band thermo-optic carbon analyzer (Zhang and Kang, 2018; Zhong et al., 2019). In this study, DRI

(a)Snow section (b)Snow sample collection

Fig. 2. Sampling site photos in winter 2018. (a) Snow section, (b) Snow sample collection.

was used to measure BC concentration in the State Key Laboratory of Cryospheric Sciences. Developed by the Desert Research Institute of the United States, the analyzer is based on thermal and optical methods to quantitatively analyze the corresponding carbon components of BC deposited on the filter membrane under different temperatures and environments. This method performed an oxidation analysis on a filter of 0.5 cm^2 under different temperature and environmental conditions. The sample was gradually heated and BC was dissipated in an oxidizing environment containing 2% oxygen. The released carbon was heated and oxidized to CO_2 (the catalyst was MnO_2), which was quantitatively detected by a non-dispersive infrared (NDIR) analyzer (Zhang and Kang, 2019).

MD in snow cover was determined by allowing the snow sample to naturally melt in the indoor laboratory. The melted snow water then was immediately filtered onto a quartz fiber membrane (Whatman QMA, d = 47 mm) with an electronic vacuum pump filter. The quartz filter membrane was sterilized at 550 °C in a muffle furnace (Tianjin SX-4-10) for 6 h before the snow sample was filtered. A microbalance (Mettler AE240) was used to weigh the quartz filter membrane before and after the snow sample was filtered. The precision of the microbalance was 0.0001 g. The results were recorded. The concentration of MD was calculated by the weight difference before and after filtration of the quartz filter membrane using the following equation:

$$H_{MD} = \frac{g_{x2} - g_{m_{x1}}}{G_{m1} - G_{m2}} \quad (1)$$

where H_{MD} is the concentration of MD; G_{m1} and G_{m2} are the weights of the snow sample before and after filtration, respectively; and g_{x1}, g_{x2} are the weights of the quartz filter membrane before and after drying, respectively.

2.4. Simulations of albedo and radiative forcing

Snow albedo was calculated by the SNow, ICe, Aerosol Radiation (SNICAR) model (Flanner et al., 2007). SNICAR is a model that integrates snow, ice, and aerosol radiation modules. Based on the optical properties of snow and ice and the two-stream approximation algorithm, a two-way stream radiative transfer solution was used to simulate the hemispherical albedo of snow and ice. The parameters of the model include the incident radiation type, solar zenith angle, surface spectral distribution, effective snow radius, snow depth and density, lower ground albedo, and impurity concentration(Flanner et al., 2007). In this study, the incident radiation type was direct radiation. The solar zenith angle was obtained using the "OSGeo China" solar altitude angle online calculator. The mid-latitude winter was selected as the surface spectral distribution. The effective snow radius and snow depth and density were obtained from the measured data. The specific measurement method is presented in Section 2.2. The default value of the lower ground albedo is 0.25 in the model. Moreover, the concentrations of impurities, including BC and MD, were measured. Section 2.3 demonstrates the specific measurement method. In this study, the pure snow albedo was simulated by the SNICAR model, where the input values of the BC and MD concentration parameters were zero. Next, the measured concentrations of BC (MD concentration set to zero) and MD (BC concentration set to zero) were input to simulate the snow albedo with BC or MD. Then, the measured concentrations of BC and MD were input at the same time to simulate the snow albedo under the combined effect of BC and MD.

The snow albedo results of pure snow, snow with BC or MD, and snow with BC + MD were simulated by SNICAR. The contributions of BC, MD, and BC + MD to the snow albedo reduction were calculated as follows:

$$C_x = \frac{SA_{pure} - SA_x}{1 - SA_x} \quad (2)$$

where C_x is the contribution of BC, MD, or BC + MD to the snow albedo reduction. SA_{pure} is the albedo of pure snow, and SA_x is the albedo of BC, MD, or BC + MD.

Then, the radiative forcing (RF) caused by BC, MD, and BC + MD was calculated as follows (Kaspari et al., 2015; Zhang et al., 2018):

$$RF = \sum_{0.325\mu m}^{1.075\mu m} E(\lambda,\theta)\left(\alpha_{(\gamma,\lambda)} - \alpha_{(\gamma,\lambda,imp)}\right)\Delta\lambda \quad (3)$$

where E is the solar radiation constant, γ is the snow optical size, λ is the wavelength (μm), θ is the solar zenith angle, α is the simulated snow albedo, and imp is the impurity containing BC or MD.

2.5. Estimation of changes in snow cover duration

Impacts of light-absorbing impurities, BC and MD, on snow melting were simulated by the model proposed by Schmale et al. (2017), which is the snow cover duration (SCD). This model considered the absorptivity of snow, incoming shortwave solar radiation obtained from local weather stations, and the number of days with the daily air temperature above 0 °C(Zhong et al., 2019).The amount of snowmelt was simulated by the equation is:

$$Melt_{snow} = N_{Tht0} \times \Delta\alpha \times SW \quad (4)$$

where $Melt_{snow}$ is the amount of snowmelt, N_{Tht0} is the number of days when the daily temperature is higher than 0 °C in the snowmelt period, Δα is the albedo reduction (the difference in albedo between clean snow and snow with BC and/or MD), and SW is the shortwave radiation.

Snow characteristics can change during the process of snow melting. In this study, high concentrations of BC and MD in urban areas had a great impact on snow melting. Beginning in the stable period, BC and MD caused the snow to melt. Therefore, we used the data from the whole snow cover period to simulate changes in the snow cover duration. We considered that this method could accurately reflect the impact of BC and MD on snow melting in urban areas. According to the data measured during snow cover days, the snow density ranged from 98 to 368 kg m^{-3}, and the snow particle size ranged from 85 to 226 μm. Each snow sample was divided into three scenarios: low-density small particle size, medium-density medium particle size, and high-density large particle size. The specific division is shown in Table 1. Furthermore, the albedo of each snow sample was simulated again. The results of snow albedo caused by snow density and particle size were different and were used in the simulation model of the snow melting time. To note, the snow depth parameter needed to be further divided into two situations by using snow water equivalent (SWE) data in the snow melting time simulation. Consequently, the snow depth parameter was not considered as a parameter for snowmelt simulation.

According to the variations in snow albedo, which were the albedo simulation results of low-density small particle size, medium-density medium particle size, and high-density large particle size, the SCD simulation results were shown as three scenarios, low, medium, and high, using Eq. (4). In other words, the low scenario was the low-density small particle size; the same principle applied to the medium and high scenarios. The shortwave radiation in winter in Harbin ranges from 100 W m^{-2} to 230 W m^{-2}, according to the China Meteorological Data Service Centre. Therefore, the shortwave radiation standard was determined to be 120 W m^{-2} in the low scenario, 170 W m^{-2} in the medium scenario, and 220 W m^{-2} in the high scenario. All parameters were guaranteed to operate at low values in the low scenario. The

Table 1
Snow effective grain sizes and snow densities used for the albedo calculation with the SNICAR model.

Description	Low scenario	Medium scenario	High scenario
Snow effective grain radius (μm)	100	150	200
Snow density (kg m^{-3})	100	180	260

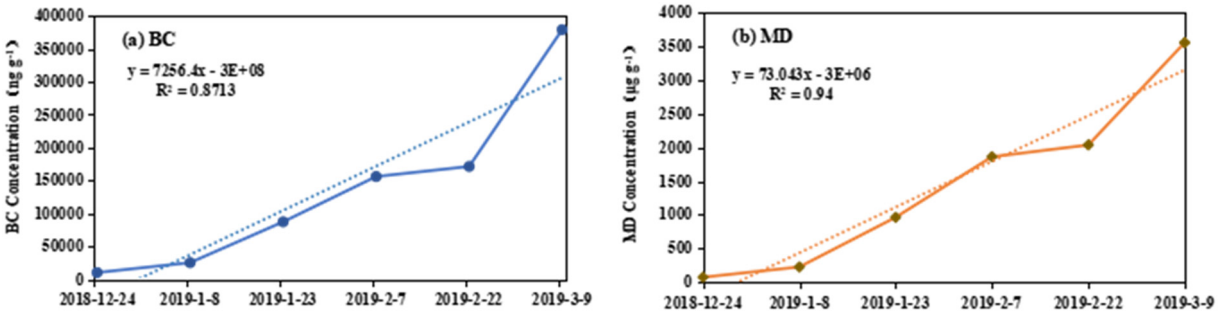

Fig. 3. Temporal variations in the concentrations of light-absorbing impurities (LAIs) on the snow surface in Harbin city during the winter of 2018. (a) Concentrations of BC (ng g^{-1}), (b) Concentrations of MD (μg g^{-1}).

medium and high scenarios drew the same analogy. Next, the SCD variations were estimated under two assumptions based on the observed SWE. According to data from the Harbin Meteorological Bureau, the SWE ranged from 28 to 86 mm during the whole snow cover period in Harbin. Hence, the study assumed that the SWE was 35 mm and 70 mm for simulation.

3. Results

3.1. Concentration distribution characteristics of BC and MD in snow cover of Harbin

Taking the whole administrative region of Harbin as an example, the average concentrations of BC and MD in snow cover of six sampling periods in Harbin ranged from 10,132.29 to 379,138.88 ng g^{-1} and 72.12 μg g^{-1} to 3552.49 μg g^{-1}, respectively. The average concentrations of BC and MD were 126,121.03 ng g^{-1} and 1419.6 μg g^{-1}, respectively. The concentrations of BC and MD in snow cover increased with time during the whole winter period (Fig. 3). The BC and MD concentrations both showed a significant increase ($P < 0.05$), which meant that the BC and MD concentrations in snow cover in Harbin increased significantly with time. The growth rate of BC concentration was greater than that of MD concentration. In the whole snow cover period, the concentrations of BC and MD during the ablation period were much higher than those in the early period, which were 30 times and 4.2 times higher, respectively, than those in the early snow period.

The distribution of BC and MD across Harbin indicated significant regional differences (Fig. 4). On the whole, average concentrations of BC and MD in Harbin during the snow cover period increased gradually from north to south. BC and MD concentrations were higher in the Xiangfang and Nangang districts than other areas. Regions with the lowest concentrations of BC and MD were located in the Hulan and Songbei districts. The reason is that the southern area is the old town of Harbin and is densely populated, with high industrial development and human activities. This led to higher levels of BC and MD concentrations.

We selected the data of snow samples on December 24, January 23, and March 9 to investigate the deposition processes of BC and MD during the early, stable, and melt periods of snow cover in Harbin (Fig. 5). Concentrations of BC and MD significantly increased from December 2018 to March 2019 across Harbin city. Although fresh snow appeared sometimes, concentrations of BC and MD still increased significantly in different periods. Concentrations of BC and MD in the snow surface of urban areas in the March 9 sampling were the highest during the whole period. Concentrations of BC and MD in the melt period reached 30 and 4.2 times that in the early period, respectively. In terms of individual districts, concentrations of BC and MD in the southern area of Harbin both increased significantly during the whole snow period. However, the values in the Hulan and Songbei districts, located in the northern Harbin, experienced much smaller changes than the Xiangfang and Nangang districts during the whole snow period.

3.2. Impacts of BC and MD on snow albedo and radiative forcing

The impacts of BC and MD on albedo reduction in 120 snow samples were simulated with the SNICAR model. Each sampling point controlled four situations in the simulation, i.e., clean snow (BC and MD concentrations were zero) and snow with BC and/or MD. The albedo of each snow

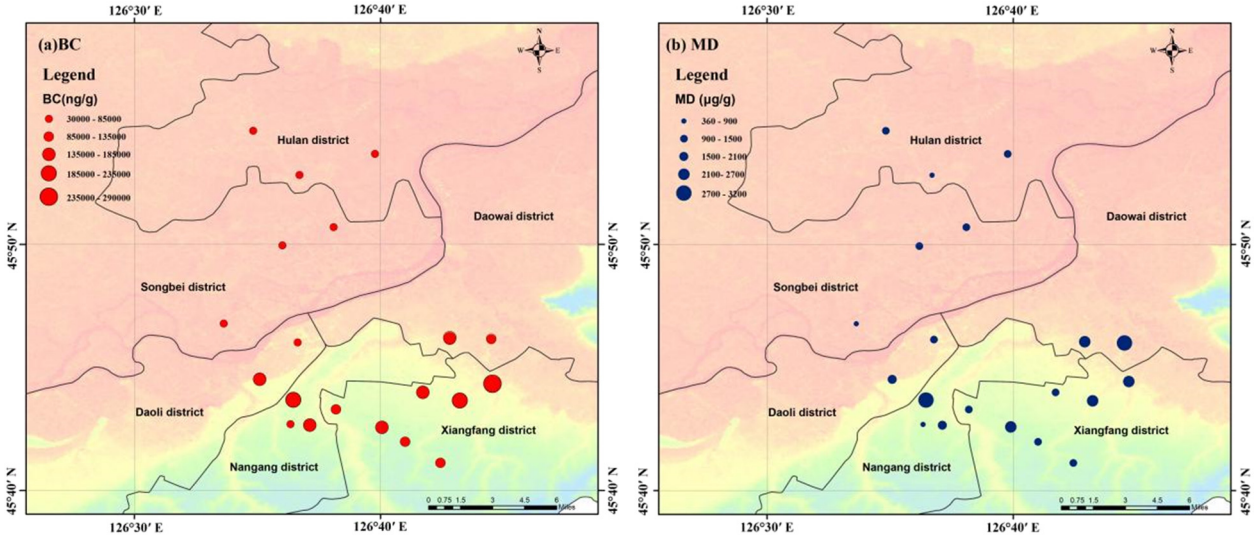

Fig. 4. Spatial distributions of average concentration of BC and MD in snow cover for sampling sites across the Harbin city during the winter of 2018.

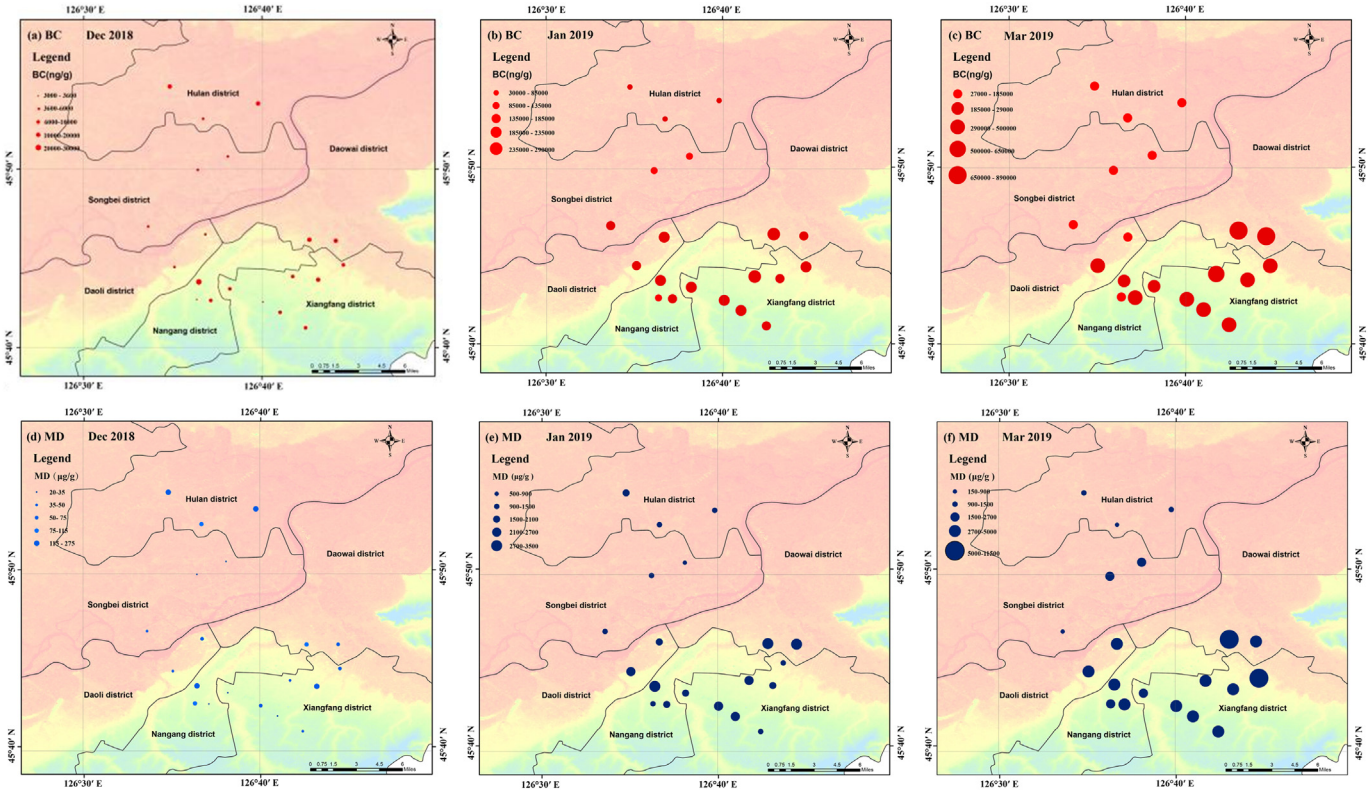

Fig. 5. Spatial distributions of BC and MD in snow cover for each sampling site during the early, stable, and melt periods of snow cover in Harbin.

sample in the four situations was obtained by simulation. The contribution rates of BC, MD, and BC + MD to the snow albedo reduction were calculated by Eq. (2). The simulation results of certain snow samples are shown in Table 2. In general, values of the average snow albedo in Harbin in the winter of 2018 were 0.7564, 0.6981, 0.3887, and 0.3841 in clean snow, snow with MD only, snow with BC only, and snow with BC and MD, respectively (Fig. 6 (a)). The contribution of BC and MD to albedo reduction was calculated as shown in Fig. 6 (b). If BC or MD was the only impurity in snow cover, the average snow albedo reduction was 0.3677 and 0.0583, respectively. The contribution of BC and MD to snow albedo reduction was 58.49% and 18.18%, respectively. The average snow albedo decreased by 0.3723 if there was BC + MD in snow cover, with contribution rate of 59.68%. The variance analysis further indicated that there were significant differences in snow albedo between snow with MD only and snow with BC + MD and snow with BC only ($P < 0.05$). Conversely, there were no significant differences in snow albedo between snow with BC + MD and snow with BC only ($P > 0.05$), indicating that BC played a major role in reducing snow albedo in Harbin.

During the sampling period, an ASD-FieldSpc4 (Analytical Spectra Devices., Inc., Boulder, United States) portable surface-object spectrometer was used to measure the snow spectral albedo, with a wavelength range of 300 to 2500 nm. The observation results of 10 sampling points were selected to verify the model. The simulated values under the condition of BC + MD were selected for verification since the observed results were the actual albedo when BC and MD coexisted in snow cover. The RMSE values were less than 10% of the observed values, with an average error of 5.84%, indicating that the results of the SNICAR model

Table 2
Sensitivity analysis of simulated albedo (SA) for BC and MD in snow cover across Harbin city using the SNICAR model.

Sample no.	Longitude	Latitude	SA			Contribution (%)			
			Clean snow	BC	MD	BC + MD	BC	MD	BC + MD
1–01	126.539	45.8262	0.6924	0.5824	0.6898	0.5811	26.35%	0.83%	26.57%
1–02	126.5604	45.7799	0.7082	0.5464	0.7024	0.5447	35.67%	1.94%	35.91%
1–03	126.5895	45.7535	0.7004	0.5474	0.6934	0.545	33.80%	2.28%	34.15%
2–01	126.539	45.8262	0.7935	0.6329	0.7919	0.6326	43.75%	0.7%	43.89%
2–02	126.5604	45.7799	0.7752	0.6647	0.7747	0.6645	32.97%	0.24%	33.50%
2–03	126.5895	45.7535	0.7131	0.4892	0.7021	0.4883	43.83%	3.68%	44.13%
3–01	126.539	45.8262	0.7961	0.3565	0.6988	0.3486	68.31%	32.31%	68.7%
3–02	126.5604	45.7799	0.8098	0.4214	0.7491	0.4203	67.19%	24.21%	68.13%
3–03	126.5895	45.7535	0.6782	0.3984	0.6649	0.3972	46.51%	3.99%	46.67%
4–01	126.539	45.8262	0.8115	0.4133	0.7058	0.4099	67.87%	35.92%	68.5%
4–02	126.5604	45.7799	0.7988	0.2949	0.6971	0.2884	71.46%	33.55%	72.46%
4–03	126.5895	45.7535	0.6962	0.2443	0.6396	0.2355	59.79%	15.69%	60.26%
5–01	126.539	45.8262	0.8157	0.4317	0.7419	0.4292	67.57%	28.59%	67.71%
5–02	126.5604	45.7799	0.8145	0.4671	0.7579	0.4669	65.20%	23.38%	65.90%
5–03	126.5895	45.7535	0.78	0.3757	0.7252	0.3727	64.77%	19.97%	64.93%
6–01	126.539	45.8262	0.8243	0.3875	0.7181	0.3814	71.31%	37.66%	71.6%
6–02	126.5604	45.7799	0.8305	0.4399	0.7662	0.4392	69.37%	27.50%	69.74%
6–03	126.5895	45.7535	0.7374	0.4333	0.6517	0.4306	53.66%	24.60%	53.88%

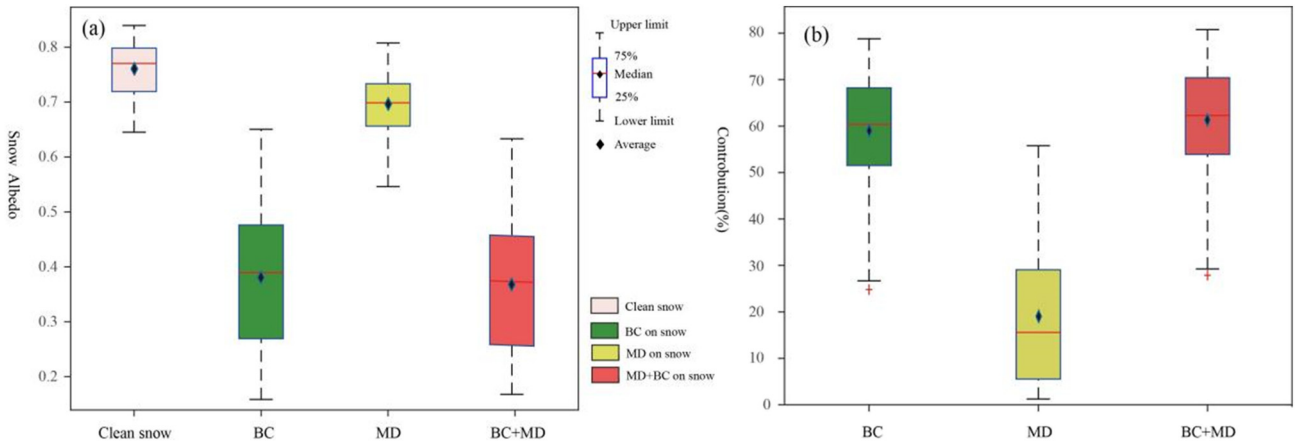

Fig. 6. (a) Average snow albedo of clean snow and snow with BC and/or MD in Harbin in winter 2018. (b) Contribution of BC and/or MD to albedo reduction of snow cover in Harbin in winter 2018.

accurately characterized the impacts of light-absorbing impurities on snow albedo reduction. Certain scholars have used the SNICAR model to simulate snow albedo and confirmed the reliability of the model through verification (Zhang et al., 2017; Li et al., 2018; Zhong et al., 2019).

According to the albedo data simulated by SNICAR, the impacts of BC, MD, and BC + MD on the RF of snow cover in Harbin were calculated by Eq. (3), as shown in Fig. 7. The RF caused by BC was 44.94 W m^{-2}. The average RF caused by MD was 7.58 W m^{-2}, and the average RF caused by BC + MD increased to 45.27 W m^{-2}. According to the variance analysis, the impacts of BC and MD on RF of snow cover displayed significant differences ($P < 0.01$). However, there were no differences in the impacts of BC and BC + MD on the radiative forcing of snow cover ($P > 0.05$). In addition, there were significant differences between MD and BC + MD on the radiative forcing of snow cover ($P < 0.01$). Hence, the impacts of BC were greater than those of MD on solar radiation absorption of snow cover in Harbin.

3.3. Changes in snow cover duration

There were three scenarios in the simulation of SCD in Harbin: the low, medium, and high scenarios. The results of Eq. (4) showed that the average SCD reduction was the largest in the low scenario, followed by the medium and high scenarios in general (Table 3). It was found in all scenarios that the SCD reduction caused by BC was greater than that caused by MD. The maximum SCD reduction caused by BC was 7.9 ± 1.16 d while that caused by MD was 3.7 ± 0.91 d. Furthermore, BC, MD, and BC + MD decreased SCD more significantly when SWE = 70 mm than when SWE = 35 mm ($P < 0.05$), revealing the light-absorbing impurities in snow cover led to SCD reduction when SWE was high.

The results showed that when SWE = 35 mm, the SCD reduction caused by BC, MD, and BC + MD ranged from 1.78 d to 4.64 d, 0.66 d to 2.43 d, and 1.8 d to 4.8 d, respectively. When SWE = 70 mm, the SCD reduction caused by BC, MD, and BC + MD increased approximately twofold. The maximum value was the reduction in SCD as a result of BC + MD, i.e., by 8.59 ± 1.3 d under the low scenario. The variance analysis showed that there were significant differences in SCD when only BC or MD was present in snow cover regardless of whether SWE = 35 mm or 70 mm ($P < 0.05$). Moreover, there were no significant differences in SCD between BC + MD and BC ($P > 0.05$). However, there were significant differences in SCD between BC + MD and MD ($P < 0.05$).

3.4. Distribution and impacts of BC and MD concentrations in different functional areas

Harbin was divided into three functional areas, the industrial area, residential area, and suburban area, to further clarify the distribution

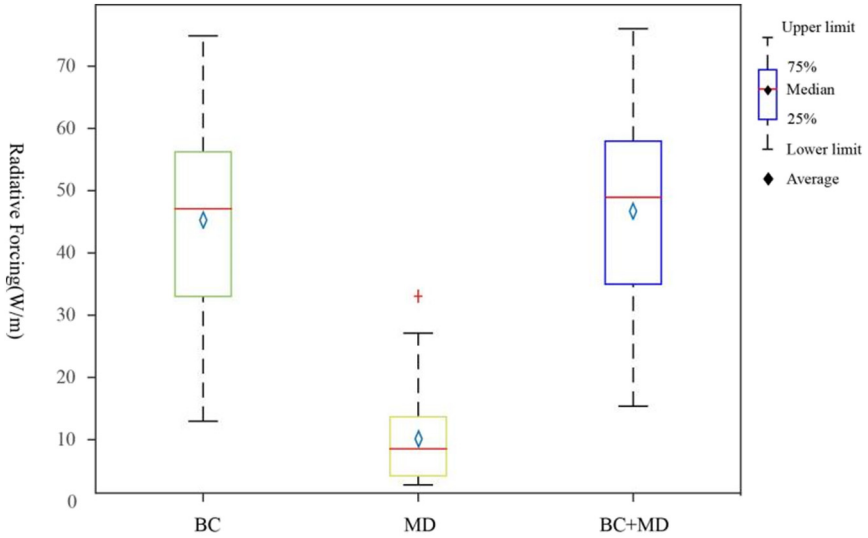

Fig. 7. Effect of radiative of forcing of BC and/or MD on albedo reduction of snow cover in Harbin in winter 2018.

Table 3
Average reduction of snow cover duration by BC and MD for different SWE values and shortwave radiation.

Scenario	Shortwave	SWE					
		SWE = 35 mm			SWE = 70 mm		
		BC	MD	BC + MD	BC	MD	BC + MD
Low scenario	SW = 120 W m^{-2}	3.96 ± 0.68	1.82 ± 0.61	4.14 ± 0.66	7.9 ± 1.16	3.7 ± 0.91	8.59 ± 1.3
Medium scenario	SW = 170 W m^{-2}	2.78 ± 0.47	1.29 ± 0.43	2.81 ± 0.47	5.57 ± 0.95	2.51 ± 0.86	5.63 ± 0.95
High scenario	SW = 220 W m^{-2}	2.15 ± 0.37	0.99 ± 0.33	2.17 ± 0.37	4.31 ± 0.74	1.99 ± 0.67	4.35 ± 0.73

Table 4
Concentration distribution of BC and MD in snow cover in different functional areas of Harbin.

Areas	Light-absorbing impurity (BC (ng g^{-1}), MD (μg g^{-1}))	Max concentration	Min concentration	Average concentration			
				Whole period	Early period	Stable period	Ablation period
Industrial	BC	794,392.48	16,734.06	211,899.02	17,099.97	292,389.35	412,374.87
	MD	11,500	113.52	2276.94	160.21	1818.18	3951.26
Residential	BC	339,080.08	4875	122,646.93	9762.75	106,530.98	281,070.66
	MD	8356.45	20.95	1338.92	35.88	1032.32	2444.16
Suburban	BC	140,695.46	1722.22	52,165.63	4704.26	66,095.51	78,140.66
	MD	4059.07	4.74	726.8	27.74	904.42	1136.11

characteristics of BC and MD concentrations in snow cover in different areas of the city and the impacts on snow albedo, radiative forcing, and snow melting.

3.4.1. Concentration characteristics of BC and MD

The concentration distribution of BC and MD in snow cover in different functional areas of Harbin is shown in Table 4. During the whole snow period, the average concentrations of BC and MD in the industrial area were the highest, followed by the residential area and suburban area. The average concentration of BC in the industrial area was 1.72 and 4.06 times higher than that in the residential area and suburban area, respectively. The average concentration of MD in the industrial area was 1.7 and 3.13 times higher than that in the residential area and suburban area. The growth rates of BC and MD concentrations in snow cover from the early period to the ablation period were the fastest in the industrial area, which were 5270.33 ng g^{-1}/d and 50.55 μg g^{-1}/d, respectively, followed by the residential area and suburban area. The growth rates of BC concentration in snow cover in the residential area and suburban area were 3617.43 ng g^{-1}/d and 797.15 ng g^{-1}/d, respectively. The growth rates of MD concentration were 32.11 μg g^{-1}/d and 14.77 μg g^{-1}/d in the residential area and suburban area, respectively. In addition, the results of variance analysis indicated that the concentration distribution of BC and MD in snow cover in the industrial area, residential area, and suburban area showed significant differences ($P < 0.05$).

3.4.2. Impacts of BC and MD on albedo and radiative forcing

1) Impacts on albedo and radiative forcing.

Table 5 displayed that BC, MD and BC + MD led to the snow albedo reduction in different functional areas, compared with clear snow. The degree of impacts were industrial area > residential area > suburban area. The snow albedo reduction by BC + MD was greater than that by BC and MD. The snow albedo reduction by MD was the smallest. The value induced by BC + MD in the industrial area was 7.3% and 15.4% greater than that in residential area and suburban area, respectively. The BC concentration in the industrial area was 6.9% and 14.7% greater than that in the residential area and suburban area, respectively. Snow albedo caused by MD was 1.9% and 3.6%, compared with that in residential area and suburban area, respectively. Similarly, the contributions of BC, MD, and BC + MD to the snow albedo reduction in different functional areas were industrial area > residential area > suburban area. Furthermore, the results of variance analysis showed that the differences of snow albedo in the industrial area with BC + MD, BC, and MD in snow cover were significant, compared with that in the suburban area ($P < 0.01$). There were significant differences between the residential area and suburban area ($P < 0.05$). However, there were no significant differences between the industrial area and residential area ($P > 0.05$) under all situations.

Based on the data analysis of the average radiative forcing of snow cover in different functional areas of Harbin, the results (Table 5) revealed that the average radiative forcing by BC increased the most from the early period to the ablation period in the industrial area, followed by the residential area and suburban area (Fig. 8.). The industrial area increased by 30.15 W m^{-2} while the suburban area increased by 14.65 W m^{-2}. Under the combined effect of BC and MD, the radiative forcing of snow cover increased from 39.17 W m^{-2} in the early period to 68.23 W m^{-2}. Under the combined effect of BC and MD, the radiative forcing ranged from 20.75 W m^{-2} to 56.55 W m^{-2} and 17.47 W m^{-2} to 42.18 W m^{-2} from early snow to old snow in the residential area and suburban area, respectively. The variance analysis explained that the radiative forcing by BC + MD and BC in snow cover in the industrial area and residential area was significantly greater than that in the suburban area ($P < 0.05$). No significant differences were found between the industrial area and residential area ($P > 0.05$). There were no significant differences caused by MD among all areas ($P > 0.05$).

3.4.3. Impacts of BC and MD on snow melting

The impacts of BC and MD in snow cover on SCD in the industrial area, residential area, and suburban area of Harbin were calculated,

Table 5
Snow albedo, contribution, and radiative forcing with BC and/or MD in different functional areas of Harbin.

Areas	SA				Contribution (%)			Radiative forcing (W m^{-2})		
	Clean snow	BC	MD	BC + MD	BC	MD	BC + MD	BC	MD	BC + MD
Suburban	0.7861	0.4928	0.7391	0.4912	37.31	5.95	37.65	36.52	6.08	37.21
Residential	0.7613	0.3897	0.6968	0.3855	45.65	8.32	45.86	45.86	8.31	47.65
Industrial	0.7611	0.3204	0.6778	0.3122	58.44	16.65	59.55	53.65	10.91	54.17

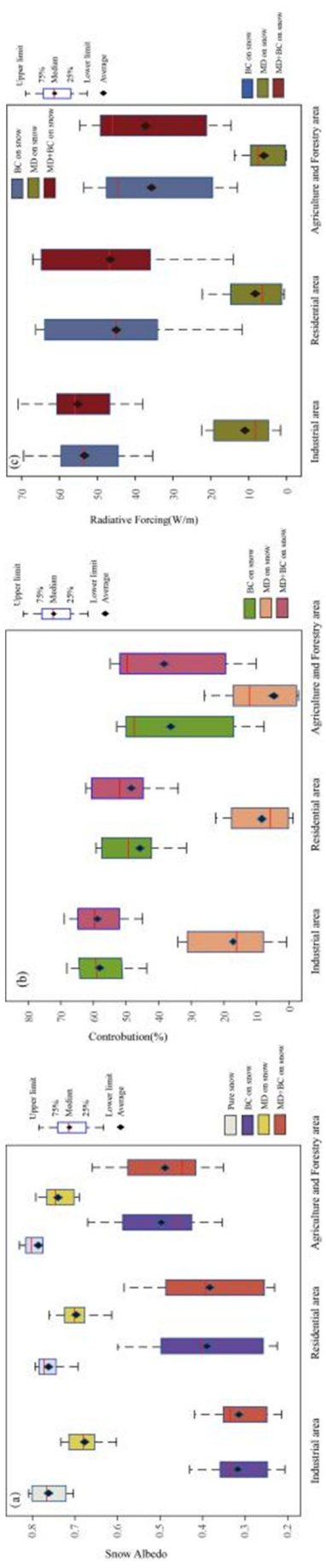

Fig. 8. (a) Average snow albedo of clean snow and snow with BC and/or MD in different functional areas of Harbin in winter 2018. (b) Contribution of BC and/or MD to albedo reduction of snow cover in different functional areas of Harbin in winter 2018. (c) Effect of radiative of forcing of BC and/or MD on albedo reduction of snow cover in different functional areas of Harbin in winter 2018.

and the results are shown in Table 6. As a whole, both BC and MD in snow cover in the three functional areas contributed to snowmelt advance under different scenarios, where the greatest effect occurred in the industrial area followed by the residential area and then the suburban area. The maximum SCD average reduction occurred in the low scenario (SW = 120 W m^{-2}), and the minimum in the high scenario in the suburban area, residential area, and industrial area. Moreover, the larger the SWE, the more the SCD decreased. When SWE was 35 mm, the average decline of SCD by BC, MD, and BC + MD in the suburban area was the smallest, with average values of 2.14 ± 0.55 d, 1.35 ± 0.71 d, and 2.17 ± 0.58 d, respectively. The contributions of BC, MD, and BC + MD to SCD reduction in the suburban area had the smallest values, reducing SCD by 1.64 ± 0.57, 0.88 ± 0.48, and 1.67 ± 0.59 d, respectively. The highest values were recorded in the industrial area where the average reduction in SCD caused by BC, MD, and BC + MD were 3.58 ± 0.11 d, 1.83 ± 0.41 d, and 3.6 ± 0.12 d, respectively, i.e., about 2.1 times those in the suburban area. BC, MD, and BC + MD in snow cover in the industrial area reduced the SCD maximum by 4.81 ± 0.18 days, 2.2 ± 0.64 d, and 4.83 ± 0.19 d, respectively. The residential area had intermediate values. When SWE was 70 mm, the SCD decrease was relatively high in the suburban area, residential area, and industrial area under all scenarios. The maximum values were simulated in the industrial area under the low scenario where the reduction in SCD caused by BC + MD was 9.66 ± 0.38 d, about 1.3 and 1.8 times that in the residential area and suburban area, respectively. According to the variance analysis, there were significant differences in SCD reduction between BC and MD and between BC + MD and MD in snow cover in the industrial area and suburban area under the low scenario ($P < 0.05$). However, no significant differences were found in the functional areas under other scenarios ($P > 0.05$).Thus, it can be seen that the SCD reduction in the industrial and suburban areas was mainly due to BC.

4. Discussion

4.1. Global concentrations of BC and MD

In the paper, BC in snow cover was measured by the thermo-optic method. For the same test method, BC concentration in snow samples in Harbin was much higher than that in other regions of the world (Table 7). For instance, BC concentration in snow cover in Harbin was 2 to 3 orders of magnitude higher than that in the North Xinjiang (Zhong et al., 2019), and was 4 to 5 orders of magnitude significantly higher than that in the Arctic and many other mid-high latitudes (Kang et al., 2020). Therefore, the concentrations of light-absorbing impurities in snow cover in urban areas with intense human interference are much higher than those in natural areas, and the impacts on snow melting are more severe. The research results of Wang et al. (2013a, 2013b) showed that BC was the main light-absorbing impurity in snow cover in the northeastern industrial area, followed by MD, consistent with this study.

4.2. Relationships between BC and MD concentrations with snow depth

The higher concentrations of BC and MD were not only related to the dry deposition of pollutants, but also related to characteristic parameters such as snow depth, density, and particle size. We analyzed the relationships between BC and MD concentrations and snow depth (Fig. 9). BC and MD concentrations increased with decreasing snow depth. There were statistically significant negative relationships of BC and MD with snow depth ($P < 0.01$), with correlation coefficients of −0.362 and − 0.414, respectively. Snow depth in Harbin during the 2018 winter was relatively low, which was also an important factor leading to the high concentrations of BC and MD. The influence of snow density and particle size on the concentrations of BC and MD should be further explored in future research.

Table 6
Average reduction of snow cover duration by BC and MD for different situations in agricultural and forestry areas, residential areas, and industrial areas.

Areas	Shortwave	SWE					
		SWE = 35 mm			SWE = 70 mm		
		BC	MD	BC + MD	BC	MD	BC + MD
Agricultural and forestry	SW = 120 W m^{-2}	2.7 ± 0.31	1.07 ± 0.83	2.73 ± 0.33	6.4 ± 0.61	2.94 ± 0.65	6.67 ± 0.65
	SW = 170 W m^{-2}	2.08 ± 0.82	1.01 ± 0.64	2.12 ± 0.82	4.16 ± 0.64	2.33 ± 0.28	4.23 ± 0.65
	SW = 220 W m^{-2}	1.64 ± 0.57	0.88 ± 0.48	1.67 ± 0.59	3.27 ± 0.15	1.75 ± 0.96	3.34 ± 0.14
	Average	2.14 ± 0.55	1.35 ± 0.71	2.17 ± 0.58	4.61 ± 0.46	2.34 ± 0.63	4.74 ± 0.48
Residential	SW = 120 W m^{-2}	3.45 ± 0.14	1.31 ± 0.5	3.49 ± 0.15	7.71 ± 0.27	2.63 ± 0.99	7.97 ± 0.31
	SW = 170 W m^{-2}	2.56 ± 0.07	1.22 ± 0.35	2.59 ± 0.08	5.12 ± 0.13	2.45 ± 0.7	5.18 ± 0.15
	SW = 220 W m^{-2}	1.97 ± 0.04	1.04 ± 0.24	2 ± 0.05	3.95 ± 0.08	2.09 ± 0.49	3.99 ± 0.09
	Average	2.66 ± 0.83	1.19 ± 0.36	2.69 ± 0.09	5.59 ± 0.16	2.39 ± 0.72	5.71 ± 0.23
Industrial	SW = 120 W m^{-2}	4.81 ± 0.18	2.2 ± 0.64	4.83 ± 0.19	9.61 ± 0.37	4.4 ± 0.88	9.66 ± 0.38
	SW = 170 W m^{-2}	3.39 ± 0.1	1.83 ± 0.34	3.41 ± 0.11	6.77 ± 0.21	3.65 ± 0.69	6.81 ± 0.22
	SW = 220 W m^{-2}	2.54 ± 0.07	1.47 ± 0.26	2.56 ± 0.07	5.08 ± 0.14	2.94 ± 0.53	5.12 ± 0.15
	Average	3.58 ± 0.11	1.83 ± 0.41	3.6 ± 0.12	7.15 ± 0.24	3.66 ± 0.7	7.19 ± 0.25

4.3. Comparison of impacts of BC and MD on albedo and radiative forcing

According to existing literature, BC and MD in snow cover in Harbin reduced snow albedo and had greater impacts on radiative forcing than in the natural area with less human disturbance. The results showed that BC and MD reduced snow albedo by 29.59% to 44.9% in Harbin. Our studies suggest that BC-induced snow darkening was significant in Harbin. This will undoubtedly have a serious impact on snowmelt and regional water availability. In addition, our results show that the average radiative forcing by BC and MD ranged from 14.03 to 69.36 W m^{-2} in the snow ablation period in spring in Harbin. The average value was 54.17 W m^{-2}, which was one to two orders of magnitude higher than those of the snow in the Arctic.

4.4. Research of impacts of BC and MD on snow cover duration

The impact of the light-absorbing impurities in snow cover on SCD was assessed. The research results of Zhong et al. (2019) on the light-absorbing impurities in snow cover in northern Xinjiang showed that the impact range of BC and MD on SCD was 1.36 ± 0.61 d to 6.12 ± 3.38 d. The combined effect of BC and MD on the Qinghai-Tibet Plateau shortened the SCD by 3.1 ± 0.1d to 4.4 ± 0.2 d. Hence, BC + MD shortened SCD in Harbin by 2 to 3 more days compared with in northern Xinjiang, and by 3 to 4 more days compared with in the Qinghai-Tibet Plateau(Zhang et al., 2018; Zhong et al., 2019). The impacts of light-absorbing impurities on snow melting in Harbin were significantly higher than those in areas with fewer human activities. In particular, the impacts of light-absorbing impurities on advanced snowmelt were very high in the industrial area. The combined effect of BC and MD decreased the SCD by 10.04 days. This paper shows that BC has a great impact on SCD in cities, especially in industrial areas. However, snow cover duration caused by BC or other factors, such as snow depth, density and grain size, needs to be further studied.

Table 7
Comparison of BC and MD concentrations in the snow of different study regions.

Region	BC (ng g^{-1})	MD (μg g^{-1})	Reference
North Ploe	5	–	Doherty et al., 2014
Canada's sub-Arctic	8	–	
Western and eastern Russia	34	–	
Svslbard	13	–	
Andes of Chile	28	–	Rowe et al., 2019
Scandinavia	88	–	Forsström et al., 2009
European Arctic and western Siberia	219	–	Evangeliou et al., 2018
Altai Mountains	2787	70	Yasunari et al., 2010
Mt. Elbrus in eastern Europe	11	–	Lim et al., 2017
North Xinjiang, China	8568	236	Zhong et al., 2019
Central and western North America	111	–	Chen et al., 2019
Alps	22	–	Gabbi et al., 2015
Cordillera Balanc Mountain	70	–	Schmitt et al., 2015
Pamir glaciers	175	–	Schmale et al., 2017
Central TP	5624	295	Zhang et al., 2017
Tianshan	3000	–	Li et al., 2017
Harbin city	126,121	1419	Our study

5. Conclusions

In this study, 120 snow samples from Harbin, a major industrial city in Northeast China, were collected from November 2018 to March 2019 to analyze the concentration distribution of BC and MD in urban snow cover and the impacts on snow albedo, radiative forcing, and snow melting. With the purpose of revealing the impacts of human disturbance, the impacts of BC and MD, which are essential light-absorbing impurities, on snow melting were analyzed in three functional areas of Harbin, the industrial area, residential area, and suburban area. The results showed the following:

(1) The concentrations of BC and MD in snow cover in Harbin ranged from 10,132.29 to 379,138.88 ng g^{-1} and 72.12 to 3552.49 μg g^{-1}, respectively, with average concentrations of 126,121.03 ng g^{-1} and 1419.6 μg g^{-1}, respectively. During the whole snow cover period, the BC concentration increased significantly ($P < 0.05$). Moreover, the growth rate of the BC concentration was significantly higher than that of MD.
(2) The average albedo of clean snow and snow with BC and/or MD in Harbin was 0.7564, 0.6981, 0.3887, and 0.3841, respectively. When BC or MD was the only impurity in snow cover, the snow albedo decreased by 0.3677 (58.49%) and 0.0583 (18.18%), respectively. When BC and MD coexisted in snow, the contribution to the average snow albedo reduction was 59.68%. The average RF by BC or MD was 44.94 W m^{-2} and 7.58 W m^{-2}, respectively. The average RF caused by BC and MD increased to 45.27 W m^{-2}.
(3) The impacts of light-absorbing impurities in Harbin on the snow melting time were mainly attributed to BC. The maximum value of advanced snowmelt by BC was 9.26 days, while that by MD was 3.75 days. Moreover, the combined effect of BC and MD advanced snowmelt by up to 8.59 ± 1.3 days.
(4) The concentrations of BC in the industrial area, residential area, and suburban area in Harbin were 211,899.02, 122,646.93, and 52,165.63 ng g^{-1}, respectively, while those of MD were 2276.94, 1338.92, and 726.8 μg g^{-1}. BC and MD in the industrial area, residential area, and suburban area reduced the average snow albedo by 0.449 (59.55%), 0.3758 (45.86%), and 0.2959 (37.65%), respectively. Furthermore, the maximum variation of radiative forcing caused by light-absorbing impurities in snow cover from the early period to the ablation period ranged from 39.17 to 68.23 W m^{-2}. Among the three functional areas, snow

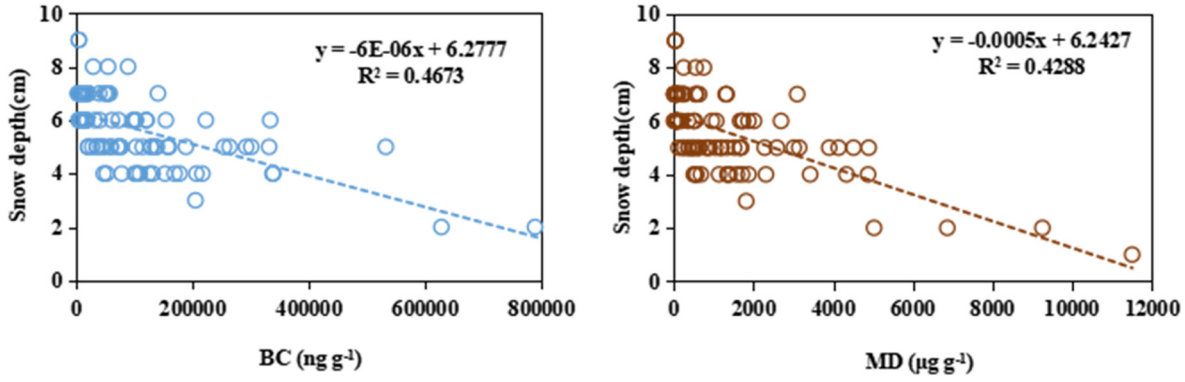

Fig. 9. Relationships between BC and MD concentrations with snow depth of Harbin.

melting was the fastest in the industrial area, followed by the residential area, and the suburban area. The maximum value was 9.66 ± 0.38 days of snowmelt advance in the industrial area under the combined effect of BC and MD. However, under the same conditions, BC + MD advanced snow melting by 7.97 ± 0.31 and 6.67 ± 0.65 days in the residential area and suburban area, respectively. Snow melting was the slowest in the suburban area, with a minimum value of MD advancing snow melting by 0.88 ± 0.48 days.

Funding

This study was supported by the National Natural Science Foundation of China (NSFC) [41771067].

CRediT authorship contribution statement

Fan Zhang was responsible for sample collection, methodology, data analysis, and put forward the research ideas of the paper and was responsible for drafting the manuscript.

Dr. Lijuan Zhang conceptualization, Methodology, Writing - Review & Editing.

Mingxi Pan was responsible for measured the contents of BC and MD in snow samples.

Xinyue Zhong provide guidance on research methods and techniques.

was responsible for downloading data and conducting statistical analysis of the downloaded data.

Enbo Zhao was responsible for the collection and processing of snow samples, and analysis of data in the laboratory.

Yifeng Wang was responsible for the collection and processing of snow samples.

Chen Du was responsible for the collection and processing of snow samples.

All contributing authors are asked to give signed consent to publication, to confirm that they have approved the final version of their manuscript and have made all required statements.

Declaration of competing interest

We declare that we have no financial and personal relationships with other people or organizations that can inappropriately influence our work, there is no professional or other personal interest of any nature or kind in any product, service and/or company that could be construed as influencing the position presented in, or the review of, the manuscript.

References

Abbatt, J.P.D., Leaitch, W.R., Aliabadi, A.A., Bertram, A.K., Blanchet, J.P., 2019. Overview paper: new insights into aerosol and climate in the Arctic. Atmos. Chem. Phys. 19 (4), 2527–2560. https://doi.org/10.5194/acp-19-2527-2019.

Ban, J., Sun, M., 2013. Causality analysis of winter precipitation anomalies in Heilongjiang province in 2012 (in Chinese). Heilongjiang Meteorol. 30 (03), 1–4.

Bo, W., Ying, W., Yongsheng, L., 2019. Characteristics of snowfall climate change in Heilongjiang Province(in Chinese). Agric. Bull. Chin. 35 (10), 114–120.

Bond, T.C., Doherty, S.J., Fahey, D.W., Forster, P.M., Berntsen, T., DeAngelo, B.J., 2013. Bounding the role of black carbon in the climate system: a scientific assessment. J. Geophys. Res. Atmos. 118 (11), 5380–5552. https://doi.org/10.1002/jgrd.50171.

Chen, L., Chow, J., Wang, X., Robles, J.A., Sumlin, B.J., Lowenthal, D.H., Zimmermann, R., Watson, J.G., 2015. Multi-wavelength optical measurement to enhance thermal/optical analysis for carbonaceous aerosol. Atmos. Meas. Tech. 8, 451–461. https://doi.org/10.5194/amt-8-451-2015.

Chen, J., Qin, X., Kang, S., Du, W., Sun, W., Liu, Y., 2019. Potential effect of black carbon on glacier mass balance during the past 55 years of laohugou glacier no.12, western Qilian Mountains. J. Earth Sci. 31 (02), 410–418. https://doi.org/10.1007/s12583-019-1238-5.

Dang, C., Warren, S.G., Fu, Q., Doherty, S.J., Sturm, M., Su, J., 2017. Measurements of light-absorbing particles in snow across the Arctic, North America, and China: effects on surface albedo. J. Geophys. Res. Atmos. 122, 10149–10168. https://doi.org/10.1002/2017JD027070.

Di Mauro, B., Fava, F., Ferrero, L., Garzonio, R., Baccolo, G., Delmonte, B., Colombo, R., 2015. Mineral dust impact on snow radiative properties in the European Alps combining ground, UAV, and satellite observations. J. Geophys. Res. Atmos. 120 (12), 6080–6097. https://doi.org/10.1002/2015JD023287.

Di Mauro, B., Baccolo, G., Garzonio, R., Giardino, C., Massabo, D., Piazzalunga, A., Rossini, M., Colombo, R., 2017. Impact of impurities and cryoconite on the optical properties of the morteratsch glacier (Swiss Alps). Cryosphere 11 (6), 2393–2409. https://doi.org/10.5194/tc-11-2393-2017.

Doherty, S.J., Dang, C., Hegg, D.A., Zhang, R.D., Warren, S.G., 2014. Black carbon and other light-absorbing particles in snow of central North America. J. Geophys. Res. Atmos. 119 (22), 12807–12831. https://doi.org/10.1002/2014JD022350.

Dombrovsky, L.A., Kokhanovsky, A.A., 2019. The influence of pollution on solar heating and melting of a snowpack. J. Quant. Spectrosc. Radiat. Transf. 241, 42–51. https://doi.org/10.1016/j.jqsrt.2019.106733.

Dou, T.F., Xiao, C.D., Du, Z.H., Schauer, J.J., Ren, H., Ge, B.Z., Xie, A.H., Tan, J.H., Fu, P.Q., Zhang, Y.X., 2017. Sources, evolution and impacts of EC and OC in snow on sea ice: a measurement study in Barrow, Alaska. Sci. Bull. 62 (22), 1547–1554. https://doi.org/10.1016/j.scib.2017.10.014.

Evangeliou, N., Schevchenko, V.P., Espen Yttri, K., Eckhardt, S., Sollum, E., Pokrovsky, O.S., Kobelev, V.O., Korobov, V.B., Lobanov, A.A., Starodymova, D.P., Vorobyev, S.N., Thompson, R., Stohl, A., 2018. Origin of elemental carbon in snow from western Siberia and northwestern european Russia during winter–spring 2014, 2015 and 2016. Atmos. Chem. Phys. 18, 963–977. https://doi.org/10.5194/acp-18-963-2018.

Flanner, M.G., Zender, C.S., Randerson, J.T., Rasch, P.J., 2007. Present-day climate forcing and response from black carbon. J. Geophys. Res. 112, D11202. https://doi.org/10.1029/2006JD008003.

Forsström, S., Ström, J., Pedersen, C.A., Isaksson, E., Gerland, S., 2009. Elemental carbon distribution in Svalbard snow. J. Geophys. Res. 114, D19112. https://doi.org/10.1029/2008JD011480.

Gabbi, J., Huss, M., Bauder, A., Cao, F., Schwikowski, M., 2015. The impact of Saharan dust and black carbon on albedo and long-term mass balance of an Alpine glacier. Cryosphere 9 (4), 1385–1400. https://doi.org/10.5194/tc-9-1385-2015.

Hansen, J., Nazarenko, L., 2004. Soot climate forcing via snow and ice albedos. Proc. Natl. Acad. Sci. U.S.A. 101, 423–428. https://doi.org/10.1073/pnas.2237157100.

He, C.L., Flanner, M.G., Chen, F., Barlage, M., Liou, K.N., Kang, S.C., Ming, J., Qian, Y., 2018. Black carbon-induced snow albedo reduction over the Tibetan plateau: uncertainties from snow grain shape and aerosol-snow mixing state based on an updated SNICAR model. Atmos. Chem. Phys. 18 (15), 11507–11527. https://doi.org/10.5194/acp-18-11507-2018.

Hu, Z.F., Kang, S.C., Li, X.F., Li, C.L., Sillanpaa, M., 2020. Relative contribution of mineral dust versus black carbon to Third Pole glacier melting. Atmos. Environ. 223, 117288. https://doi.org/10.1016/j.atmosenv.2020.117288.

Huang, J.B., Zhang, X.D., Zhang, Q.Y., Lin, Y.L., Hao, M.J., Luo, Y., Zhao, Z.C., 2017. Recently amplified arctic warming has contributed to a continual global warming trend. Nat. Clim. Chang. 7 (12), 875–879. https://doi.org/10.1038/s41558-017-0009-5.

IPCC, 2013. Technical Summary. In: Stocker, T.F., Qin, D., Plattner, G.-K., et al. (Eds.), Intergovernmental Panel on Climate Change 2013: The Physical Science Basis. Cambridge University Press, New York, USA, pp. 33–115.
Jia, H.C., Zhang, Y., Tian, S.Y., Emon, R.M., Yang, X.Y., Yan, H.R., Wu, T.T., Lu, W.C., Siddique, K.H.M., Han, T.F., 2017. Reserving winter snow for the relief of spring drought by film mulching in northeast China. Field Crop Res. 209 (1), 58–64. https://doi.org/10.1016/j.fcr.2017.04.011.
Kang, S.C., Zhang, Y.L., Qian, Y., Wang, H.L., 2020. A review of black carbon in snow and ice and its impact on the cryosphere. Earth Sci. Rev. 210, 103346. https://doi.org/10.1016/j.earscirev.2020.103346.
Kaspari, S., Skiles, S.M., Delaney, I., Dixon, D., Painter, T.H., 2015. Accelerated glacier melt on Snow Dome, Mount Olympus, Washington, USA, due to deposition of black carbon and mineral dust from wildfire. J. Geophys. Res. Atmos. 120, 2793–2807. https://doi.org/10.1002/2014JD022676.
Kuchiki, K., Aoki, T., Niwano, M., Matoba, S., Kodama, Y., Adachi, K., 2015. Elemental carbon, organic carbon, and dust concentrations in snow measured with thermal optical and gravimetric methods: variations during the 2007–2013 winters at Sapporo. Japan. J. Geophys. Res. Atmos. 120 (2), 868–882.
Li, X.F., Kang, S.C., He, X.B., Qu, B., Tripathee, L., Jing, Z.F., Paudyal, R., 2017. Light-absorbing impurities accelerate glacier melt in the central tibetan plateau. Sci. Total Environ. 587, 482–490. https://doi.org/10.1016/j.scitotenv.2017.02.169.
Li, X.F., Kang, S.C., Zhang, G.S., Qu, B., Tripathee, L., Paudyal, R., Jing, Z.F., 2018. Light-absorbing impurities in a southern tibetan plateau glacier: variations and potential impact on snow albedo and radiative forcing. Atmos. Res. 200, 77–87. https://doi.org/10.1016/j.atmosres.2017.10.002.
Li, Y., Kang, S.C., Chen, J.Z., Hu, Z.F., Wang, K., Paudyal, R., Liu, J.S., Wang, X.X., Qin, X., Sillanpaa, M., 2019. Black carbon in a glacier and snow cover on the northeastern Tibetan Plateau: concentrations, radiative forcing and potential source from local topsoil. Sci. Total Environ. 686, 1030–1038. https://doi.org/10.1016/j.scitotenv.2019.05.469.
Lim, S., Fäin, X., Ginot, P., Mikhalenko, V., Kutuzov, S., Paris, J.-D., Kozachek, A., Laj, P., 2017. Black carbon variability since preindustrial times in the eastern part of Europe reconstructed from mt. elbrus, Caucasus, ice cores. Atmos. Chem. Phys. 17, 3489–3505. https://doi.org/10.5194/acp-17-3489-2017.
Menegoz, M., Krinner, G., Balkanski, Y., Boucher, O., Cozic, A., Lim, S., Ginot, P., Laj, P., Gallee, H., Wagnon, P., 2014. Snow cover sensitivity to black carbon deposition in the Himalayas: from atmospheric and ice core measurement to regional climate simulation. Atmos. Chem. Phys. 14, 4237–4249. https://doi.org/10.5194/acp-14-4237-2014.
Ming, J., Xiao, C.D., Wang, F.T., Li, Z.Q., Li, Y.M., 2016. Grey Tienshan Urumqi Glacier No.1 and light-absorbing impurities. Environ. Sci. Pollut. Res. 23 (10), 9549–9558. https://doi.org/10.1007/s11356-016-6182-7.
Nagorski, S.A., Kaspari, S.D., Hood, E., Fellman, J.B., Skiles, S.M., 2019. Radiative forcing by dust and black carbon on the Juneau Icefield, Alaska. J. Geophys. Res. Atmos. 124 (7), 3943–3959. https://doi.org/10.1029/2018JD029411.
Niu, H.W., Kang, S.C., Zhang, Y.L., Shi, X.Y., Shi, X.F., Wang, S.J., Li, G., Yan, X.G., Pu, T., He, Y.Q., 2017. Distribution of light-absorbing impurities in snow of glacier on Mt. Yulong, southeastern Tibetan plateau. Atmos. Res. 197, 474–484. https://doi.org/10.1016/j.atmosres.2017.07.004.
Niu, H., Kang, S., Wang, H., Du, J., Pu, T., Zhang, G., Lu, X., Yan, X., Wang, S., Shi, X., 2020. Light-absorbing impurities accelerating glacier melting in southeastern tibetan plateau. Environ. Pollut. 257, 113541. https://doi.org/10.1016/j.envpol.2019.113541.
Oaida, C.M., Xue, Y.K., Flanner, M.G., Skiles, S.M., De Sales, F., Painter, T.H., 2015. Improving snow albedo processes in WRF/SSiB regional climate model to assess impact of dust and black carbon in snow on surface energy balance and hydrology over western US. J. Geophys. Res. Atmos. 120 (8), 3228–3248. https://doi.org/10.1002/2014JD022444.
Painter, T.H., Flanner, M.G., Kaser, G., Marzeion, B., VanCuren, R.A., Abdalati, W., 2013. End of the little ice age in the Alps forced by industrial black carbon. Proc. Natl. Acad. Sci. U.S.A. 110, 15216–15221. https://doi.org/10.1073/pnas.1302570110.
Paudyal, R., Kang, S.C., Tripathee, L., Guo, J.M., Sharma, C.M., Huang, J., Niu, H.W., Sun, S.W., 2019. Concentration, spatiotemporal distribution, and sources of mercury in Mt. Yulong, a remote site in southeastern Tibetan plateau. Environ. Sci. Pollut. Res. 26 (16), 16457–16469. https://doi.org/10.1007/s11356-019-05005-4.
Pu, W., Wang, X., Wei, H.L., Zhou, Y., Shi, J.S., Hu, Z.Y., Jin, H.C., Chen, Q.L., 2017. Properties of black carbon and other insoluble light-absorbing particles in seasonal snow of northwestern China. Cryosphere 11 (03), 1213–1233. https://doi.org/10.5194/tc-11-1213-2017.
Pu, W., Cui, J.C., Shi, T.L., Zhang, X.L., He, C.L., Wang, X., 2019. The remote sensing of radiative forcing by light-absorbing particles (LAPs) in seasonal snow over northeastern China. Atmos. Chem. Phys. 19 (15), 9949–9968. https://doi.org/10.5194/acp-19-9949-2019.
Qian, Y., Gustafson, J.R., Leung, L.R., Ghan, S.J., 2009. Effects of soot-induced snow albedo change on snowpack and hydrological cycle in western US based on WRF chemistry and regional climate simulations. J. Geophys. Res. 114, D03108. https://doi.org/10.1029/2008JD011039.
Qu, B., Ming, J., Kang, S.C., Zhang, G.S., Li, Y.W., Li, C.D., Zhao, S.Y., Ji, Z.M., Cao, J.J., 2014. The decreasing albedo of the zhadang glacier on western nyainqentanglha and the role of light-absorbing impurities. Atmos. Chem. Phys. 14, 11117–11128. https://doi.org/10.5194/acp-14-11117-2014.
Rowe, P.M., Cordero, R.R., Warren, S.G., Stewart, E., Doherty, S.J., Pankow, A., Schrempf, M., Casassa, G., Carrasco, J., 2019. Black carbon and other light-absorbing impurities in snow in the Chilean Andes. Sci. Rep. 9, 4008. https://doi.org/10.1038/s41598-019-39312-0.
Sadro, S., Melack, J.M., Sickman, J.O., Skeen, K.C., 2019. Limate warming response of mountain lakes affected by variations in snow. Limnol. Oceanogr. Lett. 04 (01), 9–17 (2019).
Schmale, J., Flanner, M., Kang, S., Sprenger, M., Zhang, Q., Guo, J., Li, Y., Schwikowski, M., Farinotti, D., 2017. Modulation of snow reflectance and snowmelt from central asian glaciers by anthropogenic black carbon. Sci. Rep. 7, 40501. https://doi.org/10.1038/srep40501.
Schmitt, C.G., All, J.D., Schwarz, J.P., Arnott, W.P., Cole, R.J., Lapham, E., Celestian, A., 2015. Measurements of light-absorbing particles on the glaciers in the Cordillera Blanca, Peru. Cryosphere 9 (1), 331–340. https://doi.org/10.5194/tc-9-331-2015.
Skiles, S.M., Flanner, M., Cook, J.M., Dumont, M., Painter, T.H., 2018. Radiative forcing by light-absorbing particles in snow. Nat. Clim. Chang. 8, 964–971. https://doi.org/10.1038/s41558-018-0296-5.
Svensson, J., Strom, J., Kivekas, N., Dkhar, N.B., Tayal, S., Sharma, V.P., Jutila, A., Backman, J., Virkkula, A., Ruppel, M., 2018. Light-absorption of dust and elemental carbon in snow in the Indian Himalayas and the Finnish Arctic. Atmos. Meas. Tech. 11 (3), 1403–1416. https://doi.org/10.5194/amt-11-1403-2018.
Tahir, A.A., Hakeem, S.A., Hu, T.S., Hayat, H., Yasir, M., 2019. Simulation of snowmelt-runoff under climate change scenarios in a data-scarce mountain environment. Int. J. Digit. Earth 12 (8), 910–930. https://doi.org/10.1080/17538947.2017.1371254.
Tedesco, M., Brodzik, M., Armstrong, R., Savoie, M., Ramage, J., 2009. Pan arctic terrestrial snowmelt trends (1979–2008) from spaceborne passive microwave data and correlation with the Arctic Oscillation. Geophys. Res. Lett. 36, L21402. https://doi.org/10.1029/2009GL039672.
Thind, P.S., Chandel, K.K., Sharma, S.K., Mandal, T.K., John, S., 2019. Light-absorbing impurities in snow of the Indian Western Himalayas: impact on snow albedo, radiative forcing, and enhanced melting. Environ. Sci. Pollut. Res. 26 (08), 7566–7578. https://doi.org/10.1007/s11356-019-04183-5.
Torres, C., Suarez, L., Schmitt, C., Estevan, R., Helmig, D., 2018. Measurement of light absorbing particles in the snow of the Huaytapallana glacier in the central Andes of Peru and their effect on albedo and radiative forcing. Opt. Puray Apl. 51 (04), 51004. https://doi.org/10.7149/OPA.51.4.51004.
Wang, X., Doherty, S.J., Huang, J.P., 2013a. Black carbon and other lightabsorbing impurities in snow across northern China. J. Geophys. Res. 118, 1471–1492. https://doi.org/10.1029/2012JD018291.
Wang, X., Doherty, S.J., Huang, J., 2013b. Black carbon and other light-absorbing impurities in snow across northern China. J. Geophys. Res. 118, 1471e1492. https://doi.org/10.1029/2012JD018291.
Wang, X., Wei, H.L., Liu, J., Xu, B.Q., Wang, M., Ji, M.X., Jin, H.C., 2019. Quantifying the light absorption and source attribution of insoluble light-absorbing particles on Tibetan plateau glaciers between 2013 and 2015. Cryosphere 13 (1), 309–324. https://doi.org/10.5194/tc-13-309-2019.
Warren, S.G., 2019. Light-absorbing impurities in snow: a personal and historical account. Front. Earth Sci. 6, 250. https://doi.org/10.3389/feart.2018.00250.
Wittmann, M., Zwaaftink, C.D.G., Schmidt, L.S., Gudmundsson, S., Palsson, F., Arnalds, O., Bjornsson, H., Thorsteinsson, T., Stohl, A., 2017. Impact of dust deposition on the albedo of Vatnajokull ice cap Iceland. Cryosphere 11 (2), 741–754. https://doi.org/10.5194/tc-11-741-2017.
Wu, X.J., Che, T., Li, X., Wang, N.L., Yang, X.F., 2018. Slower snowmelt in spring along with climate warming across the northern hemisphere. Geophys. Res. Lett. 45 (22), 12331–12339. https://doi.org/10.1029/2018GL079511.
Xie, X.N., Liu, X.D., Che, H.Z., Xie, X.X., Li, X.Z., Shi, Z.G., Wang, H.L., Zhao, T.L., Liu, Y.G., 2018. Radiative feedbacks of dust in snow over eastern Asia in CAM4-BAM. Atmos. Chem. Phys. 18 (17), 12683–12698. https://doi.org/10.5194/acp-18-12683-2018.
Xu, B.Q., Cao, J.J., Hansen, J., Yao, T.D., Joswia, D.R., Wang, N.L., Wu, G.J., Wang, M., Zhao, H.B., Yang, W., 2009. Black soot and the survival of Tibetan glaciers. Proc. Natl. Acad. Sci. U.S.A. 106, 22114–22118. https://doi.org/10.1073/pnas.0910444106.
Yasunari, T.J., Bonasoni, P., Laj, P., Fujita, K., Vuillermoz, E., Marinoni, A., Cristofanelli, P., Duchi, R., Tartari, G., Lau, K.-M., 2010. Estimated impact of black carbon deposition during pre-monsoon season from Nepal climate observatory-pyramid data and snow albedo changes over himalayan glaciers. Atmos. Chem. Phys. 10, 6603–6615.
Zhang, Y.L., Kang, S.C., 2018. Characteristics of carbonaceous aerosols analyzed using a multiwavelenth thermal/optical carbon analyzer: a case study in Lanzhou City. Sci. China Earth Sci. 61. https://doi.org/10.1007/s11430-017- 9245-9.
Zhang, Y., Kang, S., 2019. Characteristics of carbonaceous aerosols analyzed using a multiwavelenth thermal/optical carbon analyzer: a case study in Lanzhou City. Sci. China Earth Sci. 61. https://doi.org/10.1007/s11430-017-9245-9.
Zhang, Y.L., Kang, S.C., Cong, Z.Y., Schmale, J., Sprenger, M., Li, C.L., Yang, W., Gao, T.G., Sillanpaa, M., Li, X.F., 2017. Light-absorbing impurities enhance glacier albedo reduction in the southeastern Tibetan plateau. J. Geophys. Res. Atmos. 122 (13), 6915–6933. https://doi.org/10.1002/2016JD026397.
Zhang, Y.L., Kang, S.C., Sprenger, M., Cong, Z.Y., Gao, T.G., Li, C.L., Tao, S., Li, X.F., Zhong, X.Y., Xu, M., 2018. Black carbon and mineral dust in snow cover on the tibetan plateau. Cryosphere 12 (2), 413–431. https://doi.org/10.5194/tc-12-413-2018.
Zhao, C., Hu, Z., Qian, Y., Leung, L.R., Huang, J., Huang, M., Jin, J., Flanner, M.G., Zhang, R., Wang, H., 2014. Simulating black carbon and dust and their radiative forcing in seasonal snow: a case study over North China with field campaign measurements. Atmos. Chem. Phys. 14 (20), 11475–11491. https://doi.org/10.5194/acp-14-11475-2014.
Zhong, X.Y., Kang, S.C., Zhang, W., Yang, J.H., Li, X.F., Zhang, Y.L., Liu, Y.J., Chen, P.F., 2019. Light-absorbing impurities in snow cover across Northern Xinjiang, China. J. Glaciol. 65 (254), 940–956. https://doi.org/10.1017/jog.2019.69.
Zhong, X.Y., Kang, S.C., Zhang, W., Yang, J.H., Niu, H.W., Liu, Y.J., Guo, J.M., Li, X.F., Chen, P.F., Wang, X.X., 2021. Continuously observed light absorbing impurities in snow cover over the southern Altai Mts. in China: concentrations, impacts and potential sources. Environ. Pollut. 270, 116234. https://doi.org/10.1016/j.envpol.2020.116234.
Zhou, Y., Wang, X., Wu, X.Q., Cong, Z.Y., Wu, G.M., Ji, M.X., 2017. Quantifying light absorption of iron oxides and carbonaceous aerosol in seasonal snow across northern China. Atmosphere 8 (4), 16. https://doi.org/10.3390/atmos8040063.